A&A 423, 267–279 (2004)
DOI: 10.1051/0004-6361:200400030
© ESO 2004

Astronomy & Astrophysics

Line profile variations in WR+O binary systems

I. The code and basic predictions

L. N. Georgiev[1] and G. Koenigsberger[2]

[1] Instituto de Astronomía, Universidad Nacional Autónoma de México, México
e-mail: georgiev@astroscu.unam.mx
[2] Centro de Ciencias Físicas, Universidad Nacional Autónoma de México, México
e-mail: gloria@astroscu.unam.mx

Received 7 January 2003 / Accepted 13 January 2004

Abstract. We compute the P Cyg line profiles formed by the stellar winds of binary systems containing a Wolf-Rayet and an O-type star, incorporating the effects due to wind eclipses and wind-wind collisions. The contribution from both stellar winds to the P Cygni emission lines is modeled for different orbital phases. The opacity and the source function are calculated assuming a simplified atom and the Sobolev approximation, and the emission-line profile is calculated by exact radiative transfer through the 3D geometry wind. We analyze the cases of a P Cygni line that is formed only in the WR wind, and the case of a line formed in both the WR and the O-star winds. The line-profile variations that are predicted by this model are presented. When compared with observations, the synthetic profiles and their phase-dependent variability provide an estimate for the opening angle of the WWC shock cone and the velocity law of both stellar winds. Ultraviolet (UV) observations of the binary system γ^2 Vel are used to illustrate how the model predictions can be applied to the observational data.

Key words. line: formation – line: profiles – radiative transfer – stars: binaries: general – stars: Wolf-Rayet

1. Introduction

Massive stars are responsible for the heavy-element enrichment of the early Universe and a significant fraction of the enrichment in the present-day Universe. Their presence marks sites of recent star formation, and they are involved in such interesting observable phenomena as supernovae, massive X-ray black hole binary systems and certain classes of gamma ray bursts. Thus, a detailed understanding of these stars is most desirable and particularly the determination of their fundamental parameters such as mass, mass-loss rate and effective temperature. The most direct method for obtaining stellar masses is through the solution of the radial velocity curves in binary systems, which assumes that the spectral lines are Doppler shifted exclusively by the projected orbital motion of the stars. However, massive binaries, and especially those containing Wolf-Rayet (WR) stars, are well-known to display line-profile variability. The distortion of the line profiles can lead to fictitious RV measurements.

The two principal mechanisms that are currently believed to produce the dominant phase-dependent line profile variability are wind-wind collisions (WWC) and wind eclipses. Koenigsberger & Auer (1985) found observational evidence for both of these effects in ultraviolet (UV) spectra of 5 WR+O binary systems, concluding, however, that the effects due to wind eclipses are the dominant ones. This led them to construct a model to compute the variability under this assumption (Auer & Koenigsberger 1994), and they were able to reproduce the general trends in the observed line-profile variability of the N IV 1718 Å line in the WR+O binary system V444 Cyg. The discrepancies between the model and the observations were attributed to WWCs. However, the primary objective of these calculations was to determine the velocity law in the WR wind, using the companion O-star's continuum emission as a probe. The main conclusion of this study was that the acceleration of the WR wind occurs over larger distances than predicted by the standard β velocity laws with $\beta \leq 2$. This result is a subject of debate because, among other reasons, the model assumes that the variability results only from the absorption of O-star continuum radiation as it passes through a spherically symmetric WR wind. Massive stars have dense ($\dot{M} > 10^{-6}\ M_{\odot}\,\mathrm{yr}^{-1}$) and fast ($v_{\infty} > 1000\ \mathrm{km\,s}^{-1}$) stellar winds, and when two such winds interact, the symmetry is broken. Furthermore, the region in which the WWC occurs can itself be a source of line emission that will be observed to vary as a function of orbital phase. Hence, a complete study of the line profile variability requires a model in which the emission from both stellar winds is calculated and which includes the proper geometry and emitting characteristics of the interaction region.

Article published by EDP Sciences and available at http://www.aanda.org or http://dx.doi.org/10.1051/0004-6361:200400030

The geometry for the WWC interaction and its X-ray emitting characteristics have been the subject of numerous theoretical studies (Prilutskii & Usov 1976; Luo et al. 1990; Stevens et al. 1992; Canto et al. 1996; Myasnikov et al. 1998; Pittard & Stevens 1999; Walder et al. 1999) as well as intensive observational campaigns (see van der Hucht et al. 1991 and Moffat 2002 for an overview). However, there is as yet no simple answer to the question of what geometry should be used when modeling the line-profile emission from a WWC binary system, nor is it clear to what degree the WWC region is affecting the optical and UV emission lines (Zhekov 2002; Flores et al. 2001; Marchenko et al. 1994, 1997). The simplest models for calculating the line-profile variability assume that the WWC shock cone is responsible for a pre-specified amount of emission line flux which is superposed on a broad, underlying emission feature arising in the WR star wind (Luhrs 1995). The radiative transfer is not treated. Others recognize that the WWC shock cone that winds around the O-type star carves out a "hole" in the WR-star wind. The line profile variability is computed from this non-spherically symmetric wind, combined with an assumption for the emission arising in the WWC shock cone (Pittard & Stevens 1999; Kurosawa et al. 2002). Stevens (1993) presented a model that computes the radiative transfer through both the distorted WR-star wind and the O-star wind which is confined within the WWC shock cone. He computed the equivalent widths of the emission and absorption components of P Cygni features, and compared the results with the observations of the WN5+O6 binary V444 Cyg, finding good agreement.

In this paper, we follow the approach of Stevens (1993) and we present a model that calculates the P Cygni line profiles produced by the non-spherical wind distributions that result from the WWC. This allows a comparison with emission lines that arise in both the WR and the O-star winds. Section 2 contains the description of the model; Sect. 3, the predicted line profile variations, and their dependence on some of the stellar parameters and the shape of the WWC region; Sect. 4 presents a comparison between the model predictions and the UV observations of the WC+O binary system γ^2 Vel; and Sect. 5 presents the conclusions.

2. The model

The model contains three main and almost independent parts. The first part calculates the opacity and the source function of the line(s); the second part calculates the position and the shape of the contact discontinuity surface; and the third part performs the formal solution of the equation of radiative transfer in a 3D geometry.

2.1. Source functions and opacities

The calculation of the source function for each of the stars is initially made under the assumption that the wind has an intrinsically spherically symmetric distribution of density, temperature and velocity field. The presence of the other star is ignored.

For each wind, the velocity field $v(r)$ is assumed to obey the standard β-velocity law,

$$v(r) = V_\infty \left(1 - \frac{R_0}{r}\right)^\beta \tag{1}$$

where V_∞ is the terminal velocity of the wind and R_0 is defined by

$$R_0 = R_* \left(1 - \left(\frac{V_{\rm turb}}{V_\infty}\right)^{\frac{1}{\beta}}\right). \tag{2}$$

Here R_* is the radius of the continuum forming core and $V_{\rm turb}$ is the velocity dispersion in the wind usually called "turbulent velocity". $V_{\rm turb}$ has values in the range 100–300 km s^{-1} (Groenewegen & Lamers 1989), much higher than the sound speed in the wind and cannot be due to the real turbulence. The nature of this velocity dispersion is not clear, but it is probably related to the instabilities and shocks in the wind (Groenewegen & Lamers 1989; Lamers et al. 1999). The parameter R_0 is chosen so the wind velocity $v(r)$ is equal to $V_{\rm turb}$ at $r = R_*$ which is the innermost point considered in the code.

This velocity field, combined with the mass loss rate $\dot{M}$, defines the density distribution ρ. The continuum opacity $\chi_{\rm cont}$ is assumed to be gray and proportional to the electron density $N_{\rm e}$, which, in turn, is proportional to ρ. This assumption is equivalent to assuming the absence of a strong gradient in the degree of ionization for the major electron contributors (H and He). The continuum radiation field is calculated using a local approximated Λ operator (Olson et al. 1986) with Ng acceleration (Ng 1974; Olson et al. 1986). The test runs show that our average intensity plotted as a function of radius matches the analytical solution of Hummer & Rybicki (1971) to better than 1% error.

Lamers et al. (1987) proposed a useful characterization of the distribution of the line opacity $\chi_{\rm line}$ valid for resonance lines in stellar winds. Olson (1981) proposed an analytical estimate $\chi_{\rm line}$ for lines originated from the upper level of the resonant lines ("resonant lines of excited levels"). We combine these two analytical approaches to estimate the opacity, avoiding a very time-consuming full solution. The line source function $S_{\rm line}$ is calculated in the Sobolev approximation (Sobolev 1960) corrected for the presence of the continuum as in (Hummer & Rybicki 1985). Most of the strong UV resonance lines are doublets and we need to treat them accordingly. We calculate the source function for the doublets following Olson (1982). The tests reproduce very well the source function given by this author.

Both scattering and collisional processes are taken into account in the source function, but the parametrization of the optical depth is valid for resonance lines, so the scattering term dominates.

2.2. Shape of the contact discontinuity surface

In the second part of the code the shape of the contact discontinuity surface is calculated. There are at least two analytical solutions for the shape of these surfaces (Luo et al. 1990; Stevens et al. 1992; Canto et al. 1996). However, all of these solutions

assume that the winds have attained their terminal velocities, an assumption that may not be adequate in the case of close binary systems. That is, the winds of both stars may be still accelerating at the position of the stagnation point. Thus, we have generalized the method of Stevens et al. (1992) so as to include the possibility that the winds collide before they have reached the terminal speeds. The position of the stagnation point ($r = r_0$) is found from the numerical solution of the equation of the momentum balance along the line connecting the two stars:

$$\left[\dot{M}_1 v_1(r)\right]^{1/2} = \left[\dot{M}_2 v_2(r)\right]^{1/2} = \Re. \quad (3)$$

Following the same arithmetic as Stevens et al. (1992) and Luo et al. (1990), but with both velocities depending on the distance to the stars, we obtain a differential equation for the shape of the discontinuity surface (same as Eq. (4) of Stevens et al. 1992, but with $\Re$ depending on r). The numerical solution of this equation gives the shape of the surface. Clearly, this is a highly idealized model for the WWC region, and it probably differs significantly from that which applies to real systems. For example, Stevens et al. (1992) performed an in-depth study of the dynamics of the stellar wind and shock structure using a 2D hydrodynamics code which accounts for radiative cooling self-consistently, and found that Kelvin-Helmholtz instabilities develop whenever the wind velocities of the two stars are not equal. Furthermore, there is a rapid growth of dynamical instabilities when radiative cooling is important in the flow. The importance of cooling is characterized by the parameter χ (Stevens et al. 1992). If $\chi < 1$, the shock region is isothermal and can radiatively cool in an efficient manner. In long-period binary systems, the post shock flow will tend to be more adiabatic, although if one of the companions is a WR star, the flow along the WR wind shock will remain radiative. In eccentric systems, such as γ^2 Vel, the degree of cooling and the resultant shock structure for the WR wind will differ substantially throughout the orbit.

There are several additional factors that may influence the shape of the WWC region. Because both stars in the WR+O binary systems have radiation-driven winds, it is possible for the radiation field of the O-type star to slow the flow of the approaching WR wind before the wind-wind interaction region is reached. This potentially important mechanism is termed "radiative braking" (Owocki & Gayley 1995; Gayley et al. 1997). Hence, the WWC may occur at significantly lower wind velocities, completely modifying the geometry of the shock cone region from that derived under the assumption that both stellar winds collide at their unperturbed velocities. Furthermore, the ionization structure of the approaching stellar wind may also be modified, leading to different emission-line characteristics in the regions of the stellar wind that face the companion, compared to the unperturbed case. The calculation of these effects requires the solution of the radiative transfer in conjunction with the hydrodynamic equations, which goes beyond the scope of the present investigation. However, by comparing the observed line profiles and their variability with the theoretically predicted profiles from our simple code, the relative importance of these additional mechanisms may be determined.

Other phenomena that may be present in the stellar winds, and which we neglect, include the possible presence of inhomogeneities in the winds and Coriolis forces. The non-homogeneous nature of the winds (i.e., the so-called "blobs", Moffat et al. 1988) is believed to be due to radiative instabilities that lead to embedded shocks (Owocki & Rybicki 1991). Given the stochastic nature of the inhomogeneities, phase-dependent line profile variability is not expected to be produced by this phenomenon, unless the external irradiation modifies the source of the inhomogeneities. Coriolis forces are expected to distort the geometry of the wind-wind collision region from that which is computed under the assumption that the interaction occurs in a non-rotating reference frame. In general, the ram pressure equilibrium between the WR wind and the O-star wind is such that the shock cone wraps around the O-type star and is tilted with respect to the axis joining the two stars by an angle that, for small values of the ratio $V_{\rm orb}/V_\infty$, can be approximated with $\delta \sim \tan^{-1}(V_{\rm orb}/V_\infty)$.

Our justifications for using an idealized model for the WWC region is that, for the present calculations, the WWC is simply a boundary between the WR star and the O-star winds, and we intend to understand the way in which the radiative transfer through each of the two winds leads to line-profile variability. The potential contribution from a time-varying, line-emitting boundary may be incorporated in future studies.

2.3. Calculation of the emergent spectrum

The third part of the code performs the radiation transfer and produces the emergent spectrum. Our method differs significantly from that used by Stevens (1993), but as we shall show below, reproduces some of his results.

The flux detected by an observer is the integral of the specific monochromatic intensity that the object emits in the direction of the observer $I_\nu(\boldsymbol{n})$ over the area A of the projection of the object on the plane of the sky:

$$F_\nu = \frac{1}{D^2}\int_A I_\nu(\boldsymbol{n})\mathrm{d}A \quad (4)$$

where D is the distance to the object, $\boldsymbol{n}$ is the unit vector defining the direction to the observer, and dA is the unit surface perpendicular to $\boldsymbol{n}$.

The surface A for a binary system is the projection on the plane of the sky of a sphere that is large enough to surround the entire system, and which includes the predominant emitting regions of both winds. The integration over A is performed using a Monte-Carlo algorithm which adapts the distribution of random points inside A so that the parts of the wind with predominant emission are better sampled.

At each such point on the surface A a ray in the direction of the observer is created. This ray crosses the winds, and the emergent intensity is calculated as a formal solution of the equation of radiative transport along this ray.

Once created, the ray is divided into intervals. For any interval of the ray (Fig. 1), one can write

$$I_{\rm out}(\nu) = I_{\rm in}(\nu)\,\exp(-\tau_\nu) + \int_0^{\Delta\tau(\nu)} S(t_\nu)\,\exp(-t_\nu)\mathrm{d}\,t_\nu, \quad (5)$$

where S is the source function, $\Delta\tau(\nu)$ is the optical depth between the ends of the interval under consideration for the given

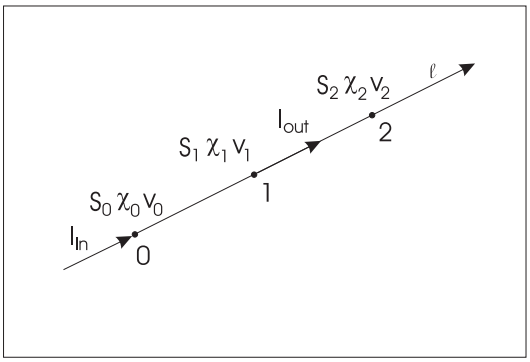

Fig. 1. Definition of the physical parameters along a line of sight used for the formal solution of the equation of radiative transport.

frequency, and $I_{\rm in}(\nu)$ and $I_{\rm out}(\nu)$ are the intensities that enter and exit the interval, respectively; i.e., the *input* and *output* intensities. At the furthermost end of the ray $I_{\rm out}(\nu) = 0$ (no incident radiation enters the system). Then Eq. (5) can be applied to the consecutive intervals until the nearest end of the ray is reached. The $I_{\rm in}(\nu)$ at this point is the emergent intensity needed for the profile calculation (Eq. (4)).

The source function and the opacity are interpolated along the ray using a monotonic cubic interpolation (Steffen 1990). The optical depth for each interval is calculated with

$$\Delta\tau(\nu) = \int_{l_0}^{l_1} \chi(l) * \phi\left(\nu - \frac{\nu_0}{c} V_z(l)\right) {\rm d}l \qquad (6)$$

where l_0 and l_1 are the coordinates along the ray at the points 0 and 1, as illustrated in Fig. 1. The integration is performed along the ray.

Once $\Delta\tau(\nu)$ is calculated, the source function $S(\tau_\nu)$ is interpolated with a quadratic polynomial $P_2(\tau)$ using the values S_0, S_1 and S_2 at the points that are numbered 0, 1 and 2 (Fig. 1).

$$\begin{aligned} S(t) \;=\; & S_0 \frac{(\tau_1 - t)(\tau_2 - t)}{(\tau_1 - \tau_0)(\tau_2 - \tau_0)} + S_1 \frac{(\tau_0 - t)(\tau_2 - t)}{(\tau_0 - \tau_1)(\tau_2 - \tau_1)} \\ & + S_2 \frac{(\tau_0 - t)(\tau_1 - t)}{(\tau_0 - \tau_2)(\tau_1 - \tau_2)}. \end{aligned} \qquad (7)$$

Substituting this into Eq. (5) $I_{\rm out}(\nu)$ adopts the form

$$I_{\rm out}(\nu) = I_{\rm in}(\nu) * \exp(-\tau_\nu) + w_o(\nu) S_0 + w_1(\nu) S_1 + w_2(\nu) S_2 \qquad (8)$$

where the S_i are the values of the source function at the points 0, 1 and 2 and the weights w_i are calculated from

$$w_k(\nu) = \int_0^{\Delta\tau(\nu)} \frac{(\tau_i - t)(\tau_j - t)}{(\tau_i - \tau_k)(\tau_j - \tau_k)} \exp(-t) {\rm d}t, \qquad i, j \neq k. \qquad (9)$$

The solution (8) can be applied for consecutive spatial intervals along a given ray. For each spatial interval, the corresponding velocity interval is calculated. The output intensity $I_{\rm out}$ is calculated and then used as the input intensity $I_{\rm in}$ for the next interval. The process starts at the boundary of the wind which is furthest from the observer, and continues step by step until the opposite boundary is reached. If the ray crosses the wind-wind collision region, then the intensity emerging from one wind is used as the boundary condition for the other wind, and the procedure is repeated except that now the velocity field and the physical conditions used correspond to those of the second wind. Thus, one can describe the process for calculating the emergent intensity along a ray in terms of "stepping" from point to point along it. At each step, the *output* intensity is calculated using the *output* intensity of the previous step as $I_{\rm in}$ and the values of S, χ and v_l at the ends of the interval.

The method has several advantages over the methods in which the emergent intensity is computed using the "common velocity surfaces (CVS)". It is purely local, and it depends only on the conditions at the points 0, 1 and 2. If the velocity field, source function and opacity do not change rapidly between these points, the solution is stable. The global geometry of the problem enters the solution only by means of the interpolation of S, χ and the projection of the velocity field.

In order to avoid a problem at the discontinuity surface, the contact discontinuity surface (CDS) is treated as a boundary. The radiative transfer along a ray is calculated independently within each of the two winds and the intensity at the CDS from one wind is treated as the boundary condition for the second wind.

The other important problem is the connection between the spatial and frequency grids introduced by the velocity field. For each spatial interval, I_ν is calculated only for the frequency interval defined by the difference of the velocities at the ends of the interval. Due to the Doppler shift between the ends of an interval along a ray, the line opacity for the rest of the frequencies is very small. If the difference between the intervals is much larger than the turbulent width of the line ($V_{\rm turb}$), the two ends of the interval are decoupled in frequency space. The resulting emission emerging from each interval becomes a Gaussian spike which barely overlaps with the emission from the previous and the next interval of the same ray. The computed emergent profile has a shape composed of these independent spikes and differs from the smooth profiles generally observed. To avoid this problem, we adapt the points along each ray so that the separation between two consecutive points along it be less than three times the turbulent velocity.

As a test, the line profiles for singlets and doublets calculated with our code were compared with those calculated by the SEI method (Lamers et al. 1987) and the results are practically identical.

3. Predicted line profile variations

Consider a WR+O binary system with a circular orbit such that the O-star is embedded in the WR wind. We will illustrate the effects on the line profiles due to the following: 1) the occultation of the O-star by the WR wind ("wind eclipse") only; and 2) wind eclipse plus the presence of a WWC shock cone that folds around the O-star. We will consider two cases: 1) the line being formed only in the WR wind; and 2) the line being formed in both winds. We will illustrate the orbital phase-dependent variations that these effects have on the line profiles. Phase $\phi = 0.0$ is defined to be when the O star is on the near side (i.e., "in front" of the WR, with respect to the observer). We will analyze 3 phases: one just after the eclipse of the WR by the O-star ($\phi = 0.05$); the second at the quadrature ($\phi = 0.25$); and the third just before the eclipse of the O-star by

Table 1. Parameters of the wind used for the test profiles.

Parameter	Value
WR wind	
$V_\infty \left[\mathrm{km\,s^{-1}}\right]$	1500 km s^{-1}
$V_{\rm turb} \left[\mathrm{km\,s^{-1}}\right]$	100 km s^{-1}
β	2.0
$\dot{M}[M_\odot/\mathrm{yr}]$	$1 \times 10^{-5}\ M_\odot$/yr
Radius	3 $R_\odot$
O wind	
$V_\infty \left[\mathrm{km\,s^{-1}}\right]$	3000 km s^{-1}
$V_{\rm turb} \left[\mathrm{km\,s^{-1}}\right]$	100 km s^{-1}
β	0.8
$\dot{M}[M_\odot/\mathrm{yr}]$	$1 \times 10^{-6}\ M_\odot$/yr
Radius	10 $R_\odot$
Orbital separation	50 $R_\odot$
Orbital velocity	120 km s^{-1}
$L_{\rm O}/L_{\rm WR}$	1.85

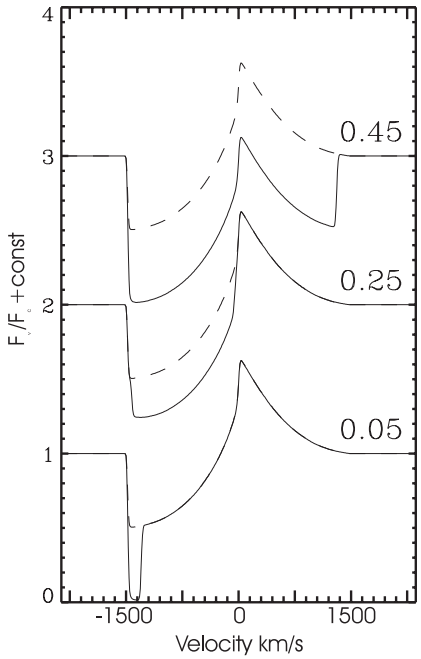

Fig. 2. Line profile variations assuming only wind eclipses. The dashed line is the profile computed for an equivalent spherically symmetric wind with no binary interaction effects. The profiles are labeled with the corresponding orbital phases.

the WR ($\phi = 0.45$). The parameters used in the test profiles are summarized in Table 1.

3.1. Line formed in the WR wind only

Consider a line that is formed in the WR wind but not in the O-star wind such as CIII] 1909 Å in WC stars. Let us assume (momentarily) that there is no interaction between the winds of the two stars. The parameters used for the lines discussed below are typical of a UV resonance line but the general conclusions are valid for any line which shows a P Cyg type profile.

The first effect on the line profile that we consider is the wind eclipse of the O-star by the WR wind, as a function of orbital phase. The predicted line-profile variations are illustrated in Fig. 2.

At $\phi = 0.05$, the portion of WR wind that lies outside of the O-star orbit, along the line-of-sight to the O-star, will produce an additional absorption in the line profile, superimposed on the intrinsic WR P Cyg absorption. Clearly, this is not a realistic situation. The space beyond the O-star orbit, along the line-of-sight to the O-star should be filled with O-star wind. But, this part of the wind is not there because we are ignoring for the moment the interaction between the two winds. This artificial feature helps to illustrate the way in which the wind eclipse affects the line profile. The blue wing of this feature is almost as extended as that of the WR star. When the O star moves in its orbit to $\phi = 0.25$ and beyond, the extra absorption extends toward the red, and starts to "eat into" the emission component, until it has extended to nearly the full width of the emission at $\phi = 0.45$. This is because the O-star is on the far side of the WR wind, and the full range of WR wind velocities is projected onto the O-star, producing absorption. At this point, the emission line is practically reduced to the continuum level. The important point to note is that the blue edge of the P Cyg absorption component never changes its velocity, remaining always at the V_∞ of the WR wind.

The emission component varies as was described by Stevens (1993) and Auer & Koenigsberger (1994) caused by the wind eclipse. When the O star is occulted by part of the WR wind, an additional absorption component decreases the contribution of the O star to the total luminosity of the system. The extent to the red of this additional absorption reflects the projected velocity of the WR wind along the line of sight to the O-star. Auer & Koenigsberger (1994) found a discrepancy between the predicted absorption (assuming only wind eclipses) and the IUE observations of V444 Cyg, and attributed this difference to the presence of the WWC.

The effects that result from the inclusion of the WWC region are illustrated in Fig. 3. The first point to note is that the O-star wind is, by construction, optically thin for the line we are considering. Thus, the WWC cone that folds around the O-star can be thought of as a "hole" in the WR's extended emitting region, thus introducing the departure from spherical symmetry. At $\phi = 0.05$, we view the WR wind through this "hole". However, because of the presence of the WWC region, the WR wind is being stopped by the O-star wind and does not achieve its terminal speed, leading to a P Cyg absorption component with a less extended blue edge than the unperturbed wind (Fig. 3, upper left panel). At $\phi = 0.15$, the absorption edge has returned to V_∞, as the "hole" moves away from the line-of-sight. At phase $\phi = 0.25$, part of the WR emission at the central wavelengths, produced in the WR wind moving perpendicular to the line-of-sight (where the "hole" is) is missing Fig. 3, upper right panel). This produces the slight decrease of the emission with respect to the same line formed in a spherically symmetric

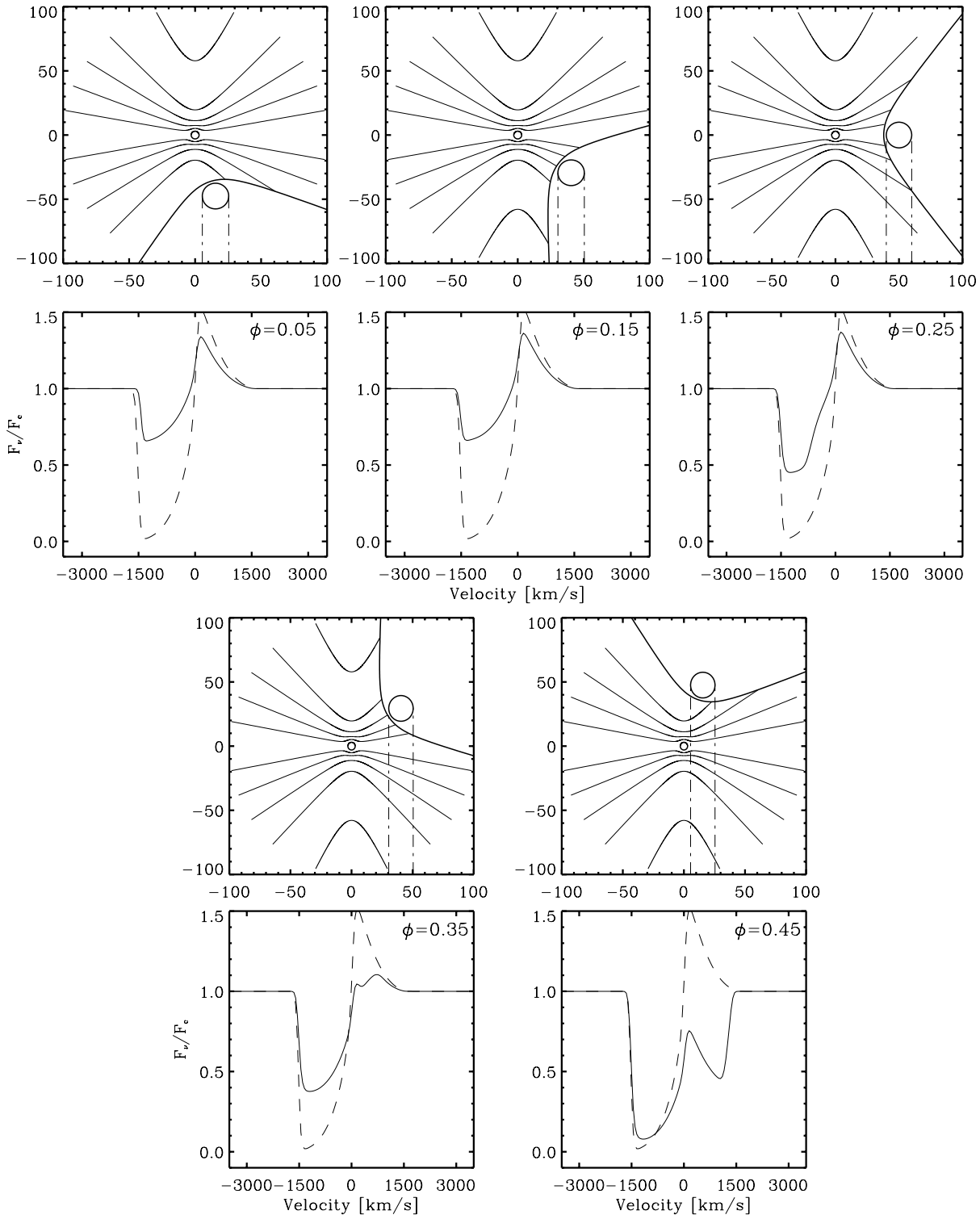

Fig. 3. Line profile variations including the effects of a WWC shock cone filled with optically thin O-star wind at different orbital phases. The corresponding common velocity surfaces, as viewed from a location perpendicular to the orbital plane, are plotted at 0.1, 0.3, 0.5, 0.7, and 0.9 V_∞. The WR star is at the origin of the coordinate system (distance in $R_\odot$) and the dot-dash lines indicate the column of wind material along the line-of-sight to the O-star from an observer located at the bottom of the page. The dashed line-profile is that produced in an equivalent, spherically symmetric wind with no binary interaction effects.

wind. The amplitude of this variation is proportional to the volume of the line forming region which is removed by the O-star wind. Part of the WR wind is projected in from of the O star. As in the case of pure wind eclipse the absorption component of the profile became deeper. At $\phi = 0.45$, the "hole" is on the back-side of the WR, and now it is the red portion of the emission line which is decreased, both in intensity (due to the absence of emitting material at these velocities) and in velocity

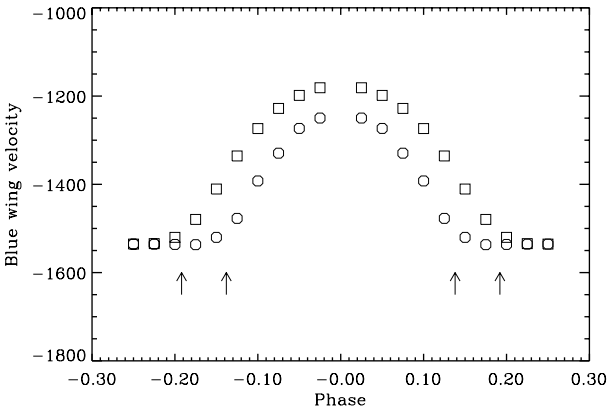

Fig. 4. The velocity of the blue wing measured at level 0.8 of the continuum for a wind having a velocity law with $\beta = 2.0$. The arrows indicate the phases at which the wall of the contact discontinuity crosses the line of sight. *Squares* – 70° opening angle; *circles* – 50°. The O-star is in front for phase 0.0.

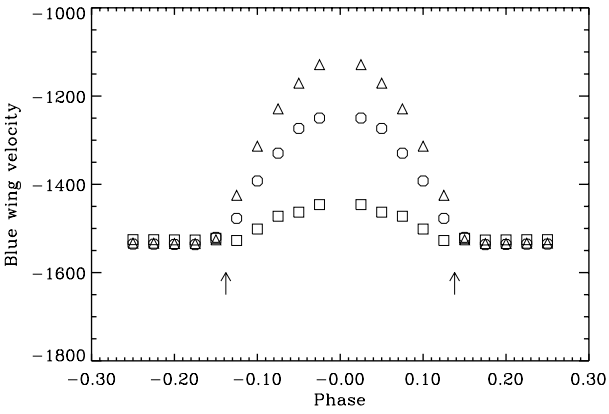

Fig. 5. The same as in Fig. 4 (50° shock cone opening angle only) but for different velocity laws. *Squares* – $\beta = 0.5$; *circles* – $\beta = 2.0$; *triangles* – $\beta = 5.0$. O star is in front for phase 0.0.

(due to the WWC region). The extent of the additional absorption is smaller than for the case without WWCR because the projection of the WR wind velocity along the line of sight to the O-star is smaller than V_∞ (Fig. 3, lower right panel). Thus, the presence of a WWC introduces phase-dependent variability in the blue edge of the P Cyg profile and decreases the intensity of the emission line red wing.

This effect was also qualitatively described by Shore & Brown (1988) for V444 Cyg and the absence of part of the dense WR wind is also inferred from the X-ray variability (Conti et al. 1995; Corcoran et al. 1996).

The degree of variability in the blue wing of the absorption component is related to the overall geometry of the contact discontinuity surface. If we assume that V_∞(WR) is not reached before the WR wind interacts with the O-star wind, the maximum velocity of the WR wind can be viewed by the observer only while the "hole" is away from the line of sight to the WR continuum-emitting core. At orbital phases when the "hole" is intersected by the the line-of-sight, the velocity of the blue wing decreases. Hence, by measuring the extent of the blue wing, and its behavior as a function of orbital phase, the opening angle of the WWC shock cone can be determined. Figure 4 shows the variation of the blue wing velocity of a line for two shock cone opening angles, 50° and 70°. The variation of the velocity is symmetric with respect to the phase 0.0. The distorsion of the CDS by other effects will lead to different variation of the velocity. If the wind is affected by radiative braking, the CDS will have larger opening angle. The changes in the velocity of the blue wing will start earlier and finish later than the case discussed above. The Coriolis force tilts the CDS. Its leading wall comes closer to the star and the trailing wall goes away from it. Therefore the changes in the blew wing velocity won't be symmetric with respect to phase $\phi = 0.0$ as above. But whatever the shape of the CDS is, it removes part of the WR wind which inevitably leads to the profile variability described above.

Furthermore, the amplitude of the variation in the blue wing of the absorption component provides information on the velocity structure of the wind. If the wind is far from achieving its terminal speed when the wind-wind collision occurs, then the observed amplitude of the variation in this wing will be large. Otherwise, it will be smaller. If the wind has already reached terminal speeds at the CDS, then no variation should be observed. Thus, the amplitude of the variability is strongly dependent on the velocity law. Figure 5 shows the dependence of the amplitude of the variability for three different velocity laws but with the same opening angle for the colliding winds shock cone. Hence, the presence of this variability indicates that the wind is still accelerating at distances where the CDS forms. Note that even if radiative braking is operating, it is not expected to affect the entire region of the wind where V_∞ has been attained, but only the regions close to the O-type star. Hence, even in this case, the above-mentioned variability should be present.

The variability of the equivalent width of the absorption component will depend on the ratio of the radii of the two stars. Consider an eclipsing system where the O-star is larger than WR. At the eclipse when the O star is in front, the absorption component of a line formed only in the WR wind will disappear, since the O star blocks the portion of the WR wind where the absorption arises. At the other eclipse, the absorption will be stronger, because there are *two* portions of WR wind material projected onto continuum sources: one in front of the WR stellar core, and the other in front of that part of the O star disk, which extends beyond the radius of the WR core. If the absorption component is seen at all phases, this means that the eclipse of the WR by the O-star is not total.

3.2. Line formed in both winds

Consider now a line which is optically thick in both winds, for example CIV 1550 Å. The profile of such a line is shown in Fig. 6. There are three major differences with respect to the previous case. First, because the O-star wind is generally faster than the WR wind, the velocity of the absorption component's blue wing is now determined mainly by the O-star wind, at all phases where this star's wind is not significantly

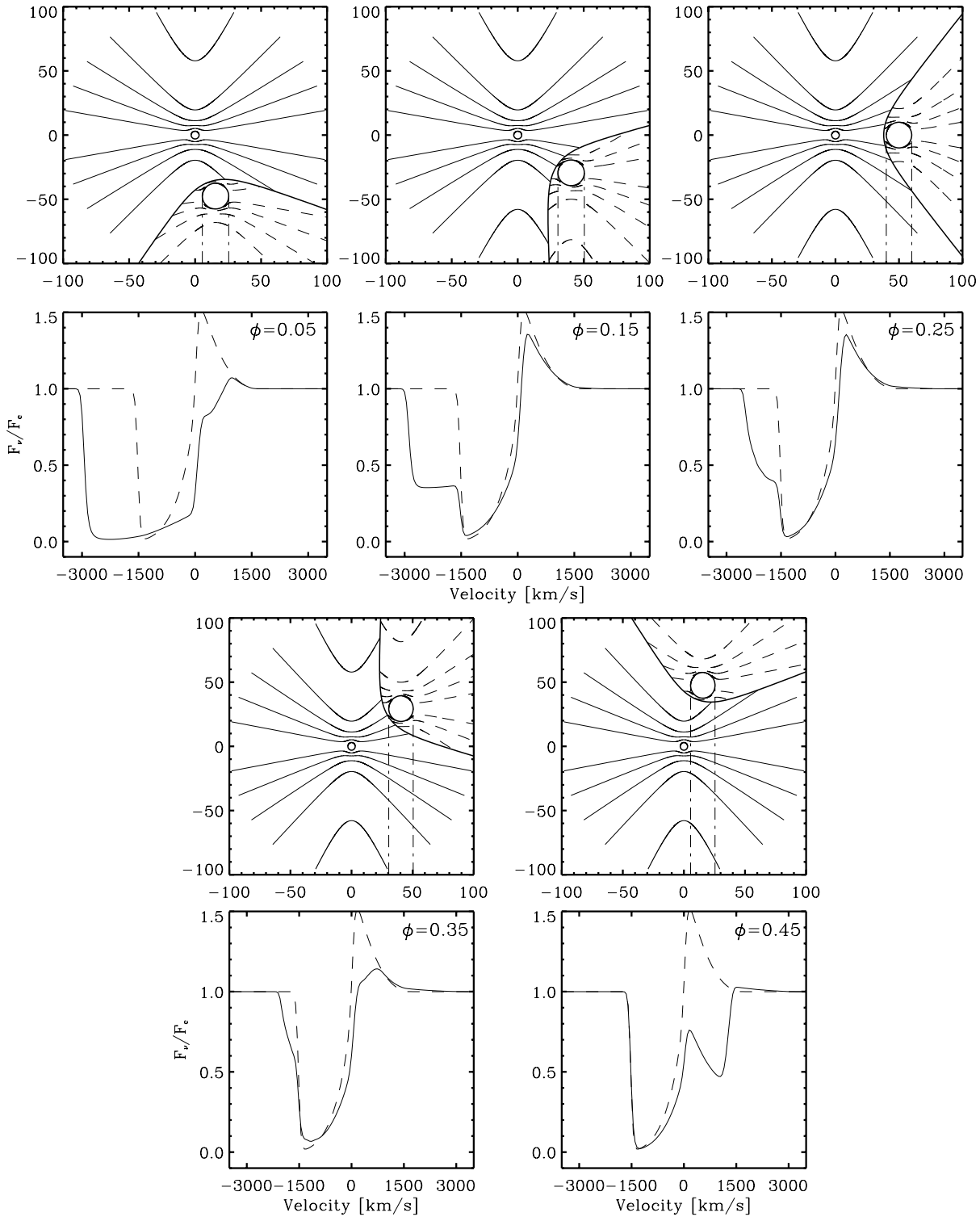

Fig. 6. Same as Fig. 3, but for the case in which the O-star wind is optically thick. Note that in this case a wind eclipse occurs near $\phi = 0$, as well as around $\phi = 0.5$.

perturbed by the WWC (Fig. 6, profiles at phases $\phi = 0.05$, $\phi = 0.15$ and $\phi = 0.25$). Thus, for velocities between $-V_\infty$(O) and $-V_\infty$(WR), only the O-star wind contributes to the absorption component. The figure shows how the maximal velocity of the O wind projected on the line of sight is reduced, which causes changes in the velocity of the blue wing of the emitted profile. For velocities lower than $-V_\infty$(WR), both winds contribute to the absorption component.

Secondly, the depth of the absorption component depends on the continuum levels of both stars in the system for velocities between $-V_\infty$(WR) and zero, but only on the continuum level of the O-star between $-V_\infty$(O) and $-V_\infty$(WR).

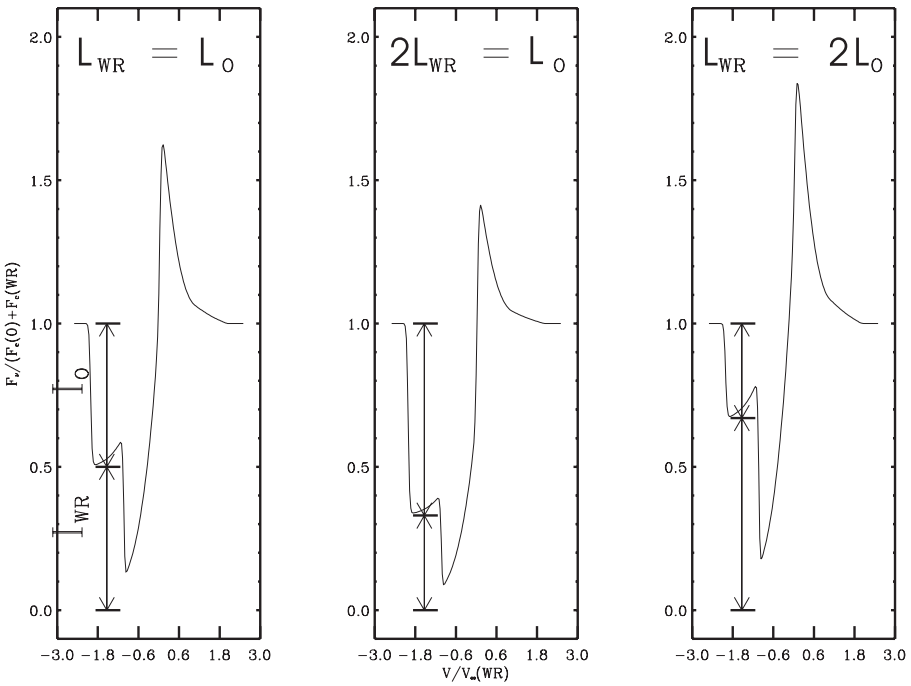

Fig. 7. Profiles of a line formed in both WR and the O-star winds at quadrature ($\phi = 0.25$) for different ratios of the continuum luminosities (indicated above the profiles). The vertical arrows mark the contributions to the P Cygni profile from each of the two stars.

Thus, a "step" is present in the P Cygni absorption component at $-V_\infty$(WR) (Fig. 6, profiles at phases $\phi = 0.15$ and $\phi = 0.25$).

And finally, we see a wind eclipse of the WR star by the O wind, which reduce the emission at the phases when the O wind is in front of the WR star (Fig. 6, upper left panel).

The effect of the "step" is illustrated in Fig. 7, where we plot P Cygni line profiles produced in three binary systems having the same wind structure, but in which the ratio between the WR and the O-star monochromatic luminosities ($L_{\rm WR}$ and $L_{\rm O}$, respectively) varies between 0.5 and 2. Similar profiles were obtained by Stevens (1993) in his model 2c. We emphasize that under the usual assumptions for the structure of stellar winds, the presence of a step in the blue wing of the P Cyg profile is a clear evidence of binarity of the object.

To quantify the phase-dependent line profile variability in this case, we measure the velocity of the P Cygni absorption component throughout an orbital cycle at two positions in its profile (illustrated by the black dots in the right panel of Fig. 8). The particular profile illustrated in Fig. 8 corresponds to an elongation in a system with V_∞(WR) = 1500 km s^{-1} and V_∞(O) = 3000 km s^{-1} and where the shock cone opening angle is 87°. The black dots are placed at fixed intensity levels of $L = 0.8$ and 0.4, with respect to the continuum level. These levels allow us to follow the behavior of the two portions of the P Cygni absorption which lie on either side of the step, when it is present. We prefer to measure the velocity at the wing of the absoption instead of often used $V_{\rm black}$. The wind of the profile is better defined in low *S/N* spectra and can be measured even for nonsaturated profiles. And also, we are interested on the variation of the velocity and not of its exact value.

The panel on the left in Fig. 8 shows how the velocities vary as a function of orbital phase. At $L = 0.4$, the O-star wind dominates when it is in front of the WR (orbital phases 0.75−1.25), while at the opposite phases, the WR-star's wind velocity dominates. The amplitude of the variation is ∼1500 km s^{-1}. The portion of the line profile at $L = 0.8$ can be attributed almost completely to the wind of the O-star, and it shows a small (200 km s^{-1}) decrease in speed around $\phi = 0.5$. This indicates that the O-star wind encounters the wind-wind collision region before it achieves its terminal velocity. Hence, Fig. 8 provides a diagnostic tool for the speed of the O-star wind just before it collides with the WR-star wind. Slower edge velocities in the C IV 1550 lines in four of the six WN+O binaries observed with the IUE by Koenigsberger & Auer (1985) at eclipse phases were interpreted as due to this effect.

3.3. Summary of predicted line-profile variations

The effects of the wind eclipse and the wind-wind interaction can be summarized as follows:

– The wind eclipse creates an additional absorption component with variable width, depending on the orbital phase. This absorption component acts to reduce the emission portion of the P Cygni profile, shifting the blue emission wing toward longer wavelengths. If the O star lies outside the WR-wind line forming region and the system is eclipsing, the emission component may disappear completely at conjunction. In non-resonance lines (particularly those observed at optical wavelengths) the effect is more subtle, and, if unaccounted for, can lead to significant distortions in the radial velocity curve of emission lines.

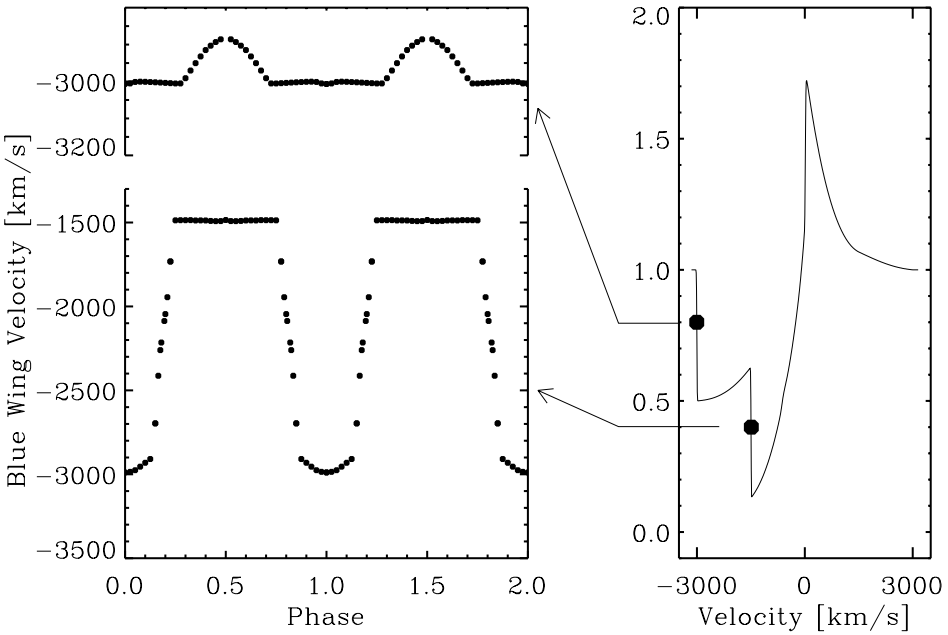

Fig. 8. *Left*: phase-dependent velocity variations of the two positions in the blue wing of a P Cygni line that is formed in both the WR and in the O-star winds. *Right*: line profile illustrating the position (black dots) where the measurements were made, and that were plotted in the left panel.

– The wind-wind interaction deforms the two winds. The O-star wind carves out a "hole" in the WR wind. Thus, the volume of WR wind on the side facing the O-star is reduced. If the "hole" extends all the way to the accelerating portion of the WR wind, then the velocity of the blue wing of the lines formed only in the WR will be variable. The amplitude of this variation provides an estimate of the WR wind velocity law. The velocity starts to deviate from the V_∞(WR) at the moment when the leading wall of the CDS crosses the line of sight and returns to V_∞(WR) when the trailing wall moves away from the line of sight. This yields a measure of the opening angle of the CDS.
If a line is formed in both winds it has a step in its blue absorption wing (Fig. 7). If the line is saturated (as CIV 1550 Å) the position of the step gives a measure of the ratio of the monochromatic luminosities of the stars at the line frequency. The wing above the step reflects the changes of the O-star wind and the wing below the step coresponds to the WR-wind. During the phases when the O-star is in front, its wind eclipses the WR star and the step disappears.
The time interval over which the velocity below the step is V_∞(O) also provides a measure of the CDS opening angle.

We emphasize that the qualitative effects described above do not depend on the detailed shape of the contact discontinuity surface. The profile variability shown will occur in any binary system where the spherical symmetry of the line-formation regions is broken, and it can be used to study the geometry of the wind regions. In particular, the current version of the code neglects the effects of the Coriolis force, which will modify the axis of symmetry of the WWC shock cone, but the tilt angle may be determined through a comparison of the predicted and the observed line-profile variability.

Table 2. Parameters of γ^2 Vel.

Parameter	Value	Refs.
$P_{\rm orb}$/days	78.5	1
e	~0.33	1
$\dot{M}_{\rm WC}/M_\odot$ yr^{-1}	2.8×10^{-5}	2
$\dot{M}_{\rm O}$	1.8×10^{-7}	3
V_∞(WC) km s^{-1}	1600	2
V_∞(O)	2500	3
$a/R_\odot$	300	1

References:
(1) Schmutz et al. (1997);
(2) De Marco & Schmutz (1999);
(3) De Marco et al. (2000).

4. Comparison with observations of γ^2 Velorum

The binary system γ^2 Vel is an eccentric and relatively long orbital period binary system containing a WC8 star and an O8 III star (Schaerer et al. 1997). The IUE archive contains 108 spectra of γ^2 Vel in the $\lambda\lambda$1200−1900 Å range, of which 93 have a good *S/N*. These spectra cover the entire orbital period of 78 days. Its orbital parameters and physical characteristics were derived by Schmutz et al. (1997); De Marco & Schmutz (1999); De Marco et al. (2000) and are reproduced here in Table 2. All velocities presented in the following sections have been corrected for the orbital motion of the WR star using the parameters from Schmutz et al. (1997).

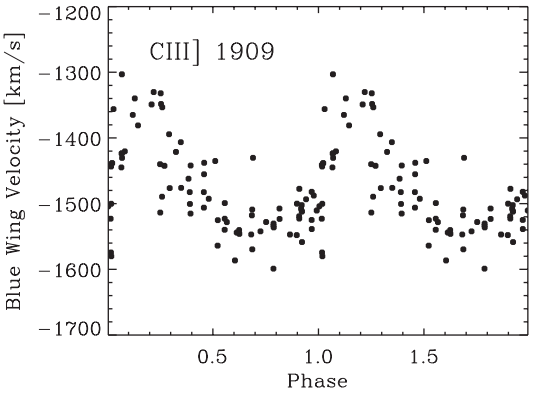

Fig. 9. The velocity of the blue wing of the absorption component of the CIII] 1909 Å line in γ^2 Vel measured at level 0.8 of the continuum. The O-star is in front at phase 0.03.

The orbital phases are defined so that the periastron passage is at phase $\phi = 0.0$. The O star is in front at phase $\phi = 0.03$ and the WR star is in front at phase $\phi = 0.61$. Note, however, that the system does not eclipse. The adopted velocities of the two winds are (De Marco & Schmutz 1999; De Marco et al. 2000) $V_\infty(\mathrm{O}) = 2500\ \mathrm{km\,s^{-1}}$ and $V_\infty(\mathrm{WR}) = 1600\ \mathrm{km\,s^{-1}}$.

4.1. Line formed in the WC8 wind only

The line C III] 1909 Å is observed only in WR stars and not in O stars. The lower level of this atomic transition is a meta-stable state, so that it can be treated as a "resonant line of excited levels". Thus, it should behave as predicted in Sect. 3.1. In Fig. 9 we plot the velocity of the "blue" wing of the P Cygni absorption component of this line, as a function of orbital phase. According to Fig. 4, the absolute value of the velocity of this feature should decrease when the O-star is in front ($\phi \sim 0.03$) if the wind-wind collision occurs in the accelerating portion of the WR wind. A change from -1550 to $-1300\ \mathrm{km\,s^{-1}}$ does occur between $\phi \sim 0.0$ and $\phi \sim 0.15$, with a return to $-1550\ \mathrm{km\,s^{-1}}$ by $\phi \sim 0.5$.

The first point to note is that the behavior of C III] requires a slow velocity law; i.e., $\beta \geq 2$, as illustrated in Fig. 5. If β were smaller, V_∞(WR) would be attained within a few stellar radii of the WR star, and, since the expected location of the WWC region lies at more than 80 R_*, no change in the C III] velocity would be measured.

The second point to note is the phase shift $\Delta\phi = 0.15$ between the observed behavior (Fig. 9) and the model prediction (Figs. 4 and 5) implying that the axis of symmetry of the shock cone is tilted with respect to the semi-major axis of the orbit.

The final point is to note that the orbital phase interval over which the variation in the C III] line occurs, which provides an estimate for the shock cone opening angle, is much larger than expected. Let us assume that the change in velocity of the line profile begins when the leading wall of the shock cone points in the direction of the observer and that the passage of the trailing wall of the shock cone marks the end of the region within which the O-star wind is constrained. Each orbital phase corresponds to an angle between the line of sight and the line connecting the two stars. This angle is equal to the true anomaly of the O-star corrected for the position of the periastron. Hence, by determining the orbital phase at which the changes in the line profile start and finish, we can derive the angles α, and β, of the shock cone walls, measured with respect to the line connecting the two stars.

In Fig. 9 the change of the C III] line velocity starts at phase 0.97 which coresponds to an angle $\alpha = 44°$. The velocity in Fig. 9 returns to V_∞(WR) at $\phi \sim 0.5$ which corresponds to an angle of $\beta \sim 160°$. The angles derived above mean that the leading wall of the CDS is closer to the star then the trailing wall. This is in agreement with the conclusion that the CDS is inclined with respect to the line connecting the two stars.

4.2. Line formed in both winds

The C IV 1548/1550 doublet, is formed in both stellar winds. In the right panel of Fig. 10 we illustrate the P Cygni profile of the CIV 1548/1550 line at orbital phase 0.788 (near elongation). The two components of this doublet are too close together to be resolved ($\Delta\lambda = 2$ Å; $\Delta V = 390\ \mathrm{km\,s^{-1}}$), so both components of the doublet contribute to the profile. The first thing to note is the presence of the "step" that is located near $-1600\ \mathrm{km\,s^{-1}}$, consistent with the value of V_∞(WR). The absorption shortward of the step location can be attributed primarily to the O-star companion, yielding $V_\infty = -2500\ \mathrm{km\,s^{-1}}$, which is consistent with previous determinations. According to Fig. 6, we can estimate the ratio of the two stars' luminosities from the "step", from which we obtain $L(\mathrm{O})/L(\mathrm{WR}) = 3$ at $\lambda 1500$ Å. This is consistent with the value of $L(\mathrm{O})/L(\mathrm{WR}) = 5.0$ obtained from optical observations by De Marco et al. (2000), assuming that the WR star is hotter than the O-star.

The panel on the left in Fig. 10 displays the velocity, as a function of orbital phase, of the blue wing of the C IV absorption line profile, at levels $L = 0.2$ and 0.85 with respect to the continuum (marked with the large black dots in the right panel of the figure). These levels were chosen so that relative changes in the velocity may be measured, and they mark the position of the line wing well below the continuum noise ($L = 0.85$) and the position below the "step" in the absorption profile ($L = 0.2$). Again we preferred this velocities instead of V_{black} due to their smaller sensitivity to the noise. The filled-in circles in Fig. 10 correspond to IUE data obtained prior to HJD 2 443 000 and the open circles to data obtained after this date. There appears to be an epoch-dependent change in the wind structure, something that has already been noted by Schmutz et al. (1997). The measured velocity of the O-star wind follows a small-amplitude ($\sim$220 $\mathrm{km\,s^{-1}}$) sinusoidal curve with a maximum near $\phi = 0.15$. We recall that velocities have been corrected for the orbital motion of the WR star. Hence, the apparent variation in the O-star's wind is simply a reflection of the relative orbital motion of the O-star with respect to the WR. There is no decrease in the wind velocity of the O-star at the phase when it is in the back of the WR ($\phi = 0.61$), as appears in the model prediction (Fig. 8) if the O-star wind collides with the WR wind before achieving V_∞(O). Hence, we are led to conclude that the wind of the O-star accelerates to V_∞(O) before the WWC occurs.

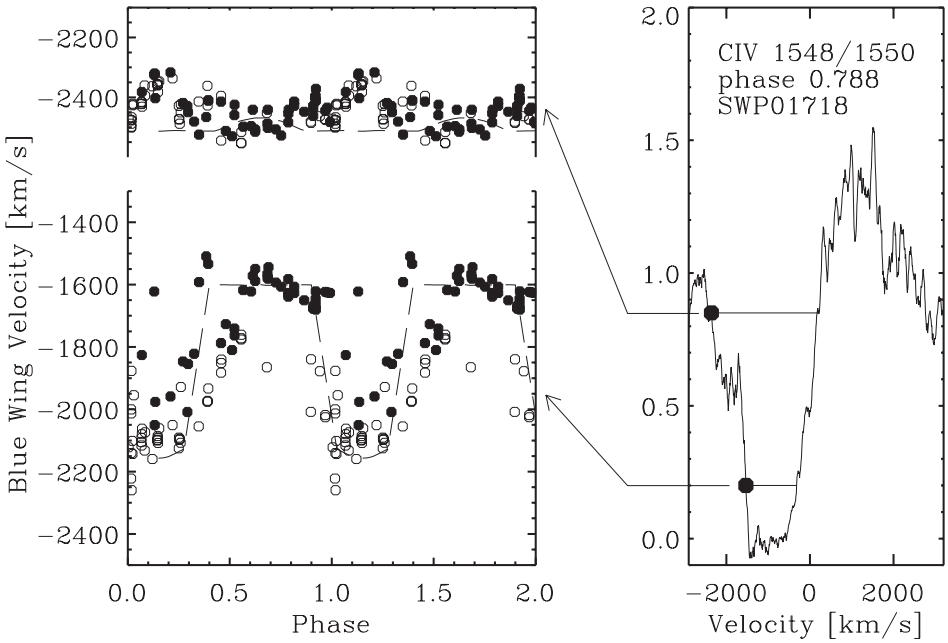

Fig. 10. *Left*: variation of the velocity of the blue wing of the CIV 1548/1550 Å doublet in γ^2 Vel, measured at two levels on the line profile, $L = 0.2$ and $L = 0.85$. The filled circles correspond to the spectra obtained before HJD 2 443 000 and the open circles to data obtained after this date. The dashes are the predicted behavior, shifted by 0.15 in phase. *Right*: line profile, plotted as a function of velocity relative to the laboratory wavelength of CIV 1548 Å at phase 0.788 and the levels at which the velocity was measured.

The velocity of the absorption profile at $L = 0.2$ undergoes a strong change between phase 0.9 ($V = -1600$ km s^{-1}) and phase 0.0 ($V = -2150$ km s^{-1}) just as predicted in Fig. 8, as the O-star wind that is emerging in the direction of the observer now also absorbs the continuum radiation from the WR star (i.e., the wind eclipse) so that its contribution to V_∞ dominates the shape of the line profile. This situation persists until $\phi = 0.3$, when the rapidly expanding O-star wind no longer occults the WR continuum emitting region, and thus, the "step" reappears in the line profile. However, instead of the variation being centered at $\phi = 0.03$ (conjunction), this variation is centered at $\phi = 0.15$. The dotted lines in Fig. 10 correspond to the model prediction, but shifted by 0.15 in phase. This result is consistent with that derived from the C III] line; i.e., the O-star wind appears to be confined within a shock cone whose leading edge is closer to the star than the trailing edge. This geometry coincides with that of a tilted shock cone, due to Coriolis forces, as discussed in Sect. 4.1, and to a larger shock cone opening angle than expected from simple WWC models.

In summary, we find that the two UV lines that were measured in γ^2 Vel undergo line profile variability that is qualitatively consistent with the predictions of the code. Specifically, during most of the the orbital cycle, the WC star's wind velocity (1600 km s^{-1}) is measurable on the C IV P Cygni absorption and a secondary absorption component belonging to the O-star (~2400 km s^{-1}) is also present; however, during a short phase interval when the O- star is in front, the only edge velocity that can be measured is that of the O-star. According to the model, this is because when the O-star wind is in front of the WR, it occults the WR continuum-emitting core and thus enhances the depth of the P Cygni absorption near V_∞(O). The main discrepancy between the observations and the model prediction lies in the implied geometry of the WWC shock cone; specifically, the shock cone opening angle is significantly larger than expected under the assumption of momentum balance and mass flux conservation. The observations also lead to the conclusion that the WWC shock cone surface is not symmetrically placed with respect to the axis of the orbit. The angle between the trailing shock cone wall and the orbital axis is larger than the corresponding angle of the leading shock cone wall, which can be understood in terms of Coriolis forces. The magnitude of the tilt angle is also larger than expected, given the wind velocities and mass-loss rates of the two stars. Both of these effects imply that the WWC occurs at WR wind velocities that are slower than V_∞(WR).

5. Summary and conclusions

This paper presents a simple numerical model that calculates the spectral line profiles emitted by winds that interact in binary systems and, through this interaction, become non-spherically symmetric. The contribution from both stellar winds to the P Cygni emission lines is modeled for different orbital phases. The opacity and the source function are calculated assuming a simplified atom and the Sobolev approximation, and the emitted profile is calculated by exact radiative transfer through the 3D geometry wind. We analyze the cases of a P Cygni line that is formed only in the WR wind, and the case of a line formed in both the WR and the O-star winds. The line-profile variations due to wind eclipses predicted by this model are similar to those computed by Stevens (1993) and Auer & Koenigsberger (1994) and the combined effect of wind eclipses plus wind-wind collisions is comparable to the results of Stevens (1993). The qualitative variability predicted by the model are also similar to the

reported UV variations in a variety of WR+O binary systems (Willis & Wilson 1976; Koenigsberger & Auer 1985; Shore & Brown 1988; St.-Louis et al. 1993; Schweickhardt et al. 1999; Setia Gunawan et al. 2001).

The principal limitations of the model are twofold: 1) we neglect interaction effects other than the wind-wind collision, such as the effects of orbital motion (Coriolis forces) radiative braking, the X-ray ionization of the stellar wind, tidal interaction effects, and the possible non-monotonic nature of the winds; and we assume these winds to be have intrinsic spherical symmetry; 2) we use a simplified model atom so that the results are applicable primarily to resonce lines and transitions in which the lower level is metastable. In exchange for these simplifications, we gain the possibility of computing the radiative transfer through both stellar winds in the colliding winds geometry at low computing costs, allowing an evaluation of the main effects produced by the wind-wind collision. The presented code, though simple, shows the main effects of the presence of the wind-wind interaction. The correct interpretation of the effects provides a tool for studying the size and shape of the contact discontinuity surface and the velocity field in the winds. The qualitative effects presented in this paper do not depend on the detailed geometry of the interaction region, and thus a simple shape of the contact discontinuity surface was chosen. Once a more detailed theoretical description of the WWC region becomes available, and "radiative braking" and Coriolis forces are incorporated, the observed line-profiles may be more precisely fit by the model. This will then provide a powerful tool for studying the properties of the stellar winds within binary systems.

Acknowledgements. We thank Jorge Cantó and Svet Zhekov for many illuminating discussions, and an anonymous referee for suggesting important improvements to this paper. This work was supported by the DGAPA project IN113999, IN118202 and CONACYT 36359, 34522-E.

References

Auer, L. H., & Koenigsberger, G. 1994, ApJ, 436, 859
Canto, J., Raga, A. C., & Wilkin, F. P. 1996, ApJ, 469, 729
Conti, P. S., Hanson, M. M., Morris, P. W., Willis, A. J., & Fossey, S. J. 1995, ApJ, 445, L35
Corcoran, M. F., Stevens, I. R., Pollock, A. M. T., et al. 1996, ApJ, 464, 434
De Marco, O., & Schmutz, W. 1999, A&A, 345, 163
De Marco, O., Schmutz, W., Crowther, P. A., et al. 2000, A&A, 358, 187
Flores, A., Auer, L. H., Koenigsberger, G., & Cardona, O. 2001, ApJ, 563, 341
Gayley, K. G., Owocki, S. P., & Cranmer, S. R. 1997, ApJ, 475, 786
Groenewegen, M. A. T., & Lamers, H. J. G. L. M. 1989, A&AS, 79, 359
Hummer, D. G., & Rybicki, G. B. 1971, MNRAS, 152, 1
Hummer, D. G., & Rybicki, G. B. 1985, ApJ, 293, 258
Koenigsberger, G., & Auer, L. H. 1985, ApJ, 297, 255
Kurosawa, R., Hillier, D. J., & Pittard, J. M. 2002, A&A, 388, 957
Lamers, H. J. G. L. M., Cerruti-Sola, M., & Perinotto, M. 1987, ApJ, 314, 726
Lamers, H. J. G. L. M., Haser, S., de Koter, A., & Leitherer, C. 1999, ApJ, 516, 872
Luhrs, S. 1995, in IAU Symp., 163, 416
Luo, D., McCray, R., & Mac Low, M. 1990, ApJ, 362, 267
Marchenko, S. V., Moffat, A. F. J., & Koenigsberger, G. 1994, ApJ, 422, 810
Marchenko, S. V., Moffat, A. F. J., Eenens, P. R. J., et al. 1997, ApJ, 485, 826
Moffat, A. 2002, Interacting winds from massive stars, in ASP Conf. Ser., 260, 3
Moffat, A. F. J., Drissen, L., Lamontagne, R., & Robert, C. 1988, ApJ, 334, 1038
Myasnikov, A. V., Zhekov, S. A., & Belov, N. A. 1998, MNRAS, 298, 1021
Ng, K. C. 1974, J. Chem. Phys., 61, 2680
Olson, G. L. 1981, ApJ, 245, 1054
Olson, G. L. 1982, ApJ, 255, 267
Olson, G. L., Auer, L. H., & Buchler, J. R. 1986, J. Quant. Spectr. Radiat. Trans., 35, 431
Owocki, S. P., & Gayley, K. G. 1995, ApJ, 454, L145
Owocki, S. P., & Rybicki, G. B. 1991, ApJ, 368, 261
Pittard, J. M., & Stevens, I. R. 1999, in Wolf-Rayet phenomena in massive stars and starburst galaxies, IAU Symp., 193, 386
Prilutskii, O. F., & Usov, V. V. 1976, Sov. Astron., 20, 2
Schaerer, D., Schmutz, W., & Grenon, M. 1997, ApJ, 484, L153
Schmutz, W., Schweickhardt, J., Stahl, O., et al. 1997, A&A, 328, 219
Schweickhardt, J., Schmutz, W., Kaufer, A., Stahl, O., & Wolf, B. 1999, in Wolf-Rayet phenomena in massive stars and starburst galaxies, IAU Symp., 193, 98
Setia Gunawan, D. Y. A., van der Hucht, K. A., Williams, P. M., et al. 2001, A&A, 376, 460
Shore, S. N., & Brown, D. N. 1988, ApJ, 334, 1021
Sobolev, V. V. 1960, Moving envelopes of stars (Cambridge: Harvard University Press)
St.-Louis, N., Moffat, A. F. J., Lapointe, L., et al. 1993, ApJ, 410, 342
Steffen, M. 1990, A&A, 239, 443
Stevens, I. R. 1993, ApJ, 404, 281
Stevens, I. R., Blondin, J. M., & Pollock, A. M. T. 1992, ApJ, 386, 265
van der Hucht, K. A., Williams, P. M., Pollock, A. M. T., et al. 1991, in Wolf-Rayet stars and interrelations with other massive stars in galaxies, IAU Symp., 143, 251
Walder, R., Folini, D., & Motamen, S. M. 1999, in Wolf-Rayet phenomena in massive stars and starburst galaxies, IAU Symp., 193, 298
Willis, A. J., & Wilson, R. 1976, A&A, 47, 429
Zhekov, S. 2002, in ASP Conf. Ser., 260, 615